Conjugated metal–organic macrocycles: Synthesis, characterization, and electrical conductivity

Leo B. Zasada,[†] Lorenzo Guio,[‡] Austin A. Kamin,[†] Diwash Dhakal,[‡] Madison Monahan,[†] Gerald T. Seidler,[§] Christine K. Luscombe,[†‡‖] and Dianne J. Xiao.[†,*]

[†] Department of Chemistry, [‡]Department of Materials Science and Engineering, and [§]Department of Physics, University of Washington, Seattle, Washington 98195, United States

[‖] Okinawa Institute of Science and Technology Graduate University, Onna-son, Okinawa 904-0495, Japan

ABSTRACT: The dimensional reduction of solids into smaller fragments provides a route to achieve new physical properties and gain deeper insight into the extended parent structures. Here, we report the synthesis of CuTOTP-OR (TOTP^{n-} = 2,3,6,7-tetraoxidotriphenylene), a family of copper-based macrocycles that resemble truncated fragments of the conductive 2D metal–organic framework $Cu_3(HHTP)_2$ (HHTP = 2,3,6,7,10,11-hexahydroxytriphenylene). The planar metal–organic macrocycles self-assemble into ordered nanotubes with internal diameters of ~2 nm and short interlayer distances of ~3.20 Å. Strong π–π stacking interactions between macrocycles facilitate out-of-plane charge transport, and pressed pellet conductivities as high as $2(1)\times10^{-3}$ S cm^{-1} are observed. Peripheral alkyl functionalization enhances solution processability and enables the fabrication of thin-film field-effect transistor devices. Ambipolar charge transport is observed, suggesting similar behavior may be operative in $Cu_3(HHTP)_2$. By coupling the attractive features of metal–organic frameworks with greater processability, these macrocycles enable facile device integration and a more nuanced understanding of out-of-plane charge transport in 2D conductive metal–organic frameworks.

Introduction. By facilitating rapid electronic, ionic, and molecular transport, nanoporous conductors enable key technologies, including electrochemical energy storage and conversion,[1–3] chemical sensing,[4,5] and electrochemically driven molecular separations.[6,7] Electrically conductive metal–organic frameworks (MOFs) are a rapidly emerging class of nanoporous conductors with excellent chemical tunability, high surface areas, and exciting charge transport behavior.[8] However, metal–organic frameworks are typically isolated as brittle and poorly dispersible microcrystalline powders, presenting significant challenges to thin film fabrication and device integration.[5] This stands in contrast to established organic semiconductors, which are compatible with scalable and low-cost solution-based processing methods.[9,10] Beyond these practical considerations, existing conductive MOFs also lack the emerging multifunctional materials properties of semiconducting polymers, including stretchability[11–13] and the ability to self-heal.[14,15]

Coupling the attractive porosity, molecular tunability, and electrical conductivity of metal–organic frameworks with the advantageous physical properties of soft matter would open the door to diverse new applications and processing methods.[16] Toward this goal, we are pursuing the dimensional reduction of electrically conductive, triphenylene-based 2D metal–organic frameworks into discrete, hexagonal macrocycles. The planar macrocyclic core should favor the formation of π-stacked structures that preserve out-of-plane charge transport and large interior channels, while the richly tunable exterior can be modified to enhance solubility and alter surface properties.

The self-assembly of rigid, shape-persistent organic macrocycles into tubular structures with nanoscale pores is well-studied, and such materials have been investigated for organic electronics, molecular recognition, and ion transport applications.[17–22] A rich diversity of organic reactions have been successfully applied to macrocycle synthesis, including C–C cross-coupling, olefin and alkyne metathesis, and amide, imine, and boronate ester formation.[20,23,24] In contrast, the use of coordination chemistry, rather than organic chemistry, to construct rigidly planar, fully conjugated metal–organic macrocycles has been less explored. Many Pd and Pt-based macrocycles have been reported,[25–28] and interesting phase behavior,[29,30] photophysical properties,[31] and biological activity[32] have been observed. However, the exploration of non-noble metal scaffolds remains relatively rare.

Here, we report the synthesis and characterization of CuTOTP-OR (TOTP^{n-} = 2,3,6,7-tetraoxidotriphenylene, R = linear C2, C4, C6, and C18 alkyl chains), a family of conjugated, copper-based metal–organic macrocycles. The planar structures self-assemble to form ordered, electrically conductive nanochannels. Average pellet conductivities of $2(1)\times10^{-3}$ S cm^{-1} are observed in CuTOTP-OC2, the shortest alkyl chain variant. Longer alkyl chain variants such as CuTOTP-OC18 readily disperse in organic solvents, facilitating the fabrication of thin-film field-effect transistor (FET) devices. Ambipolar charge transport is observed, with electron and hole mobilities on the order of ~10^{-3} cm^2 V^{-1} s^{-1}. Together, these findings show that a simple macrocyclic core can replicate key physical properties of metal–organic frameworks while affording greater processability.

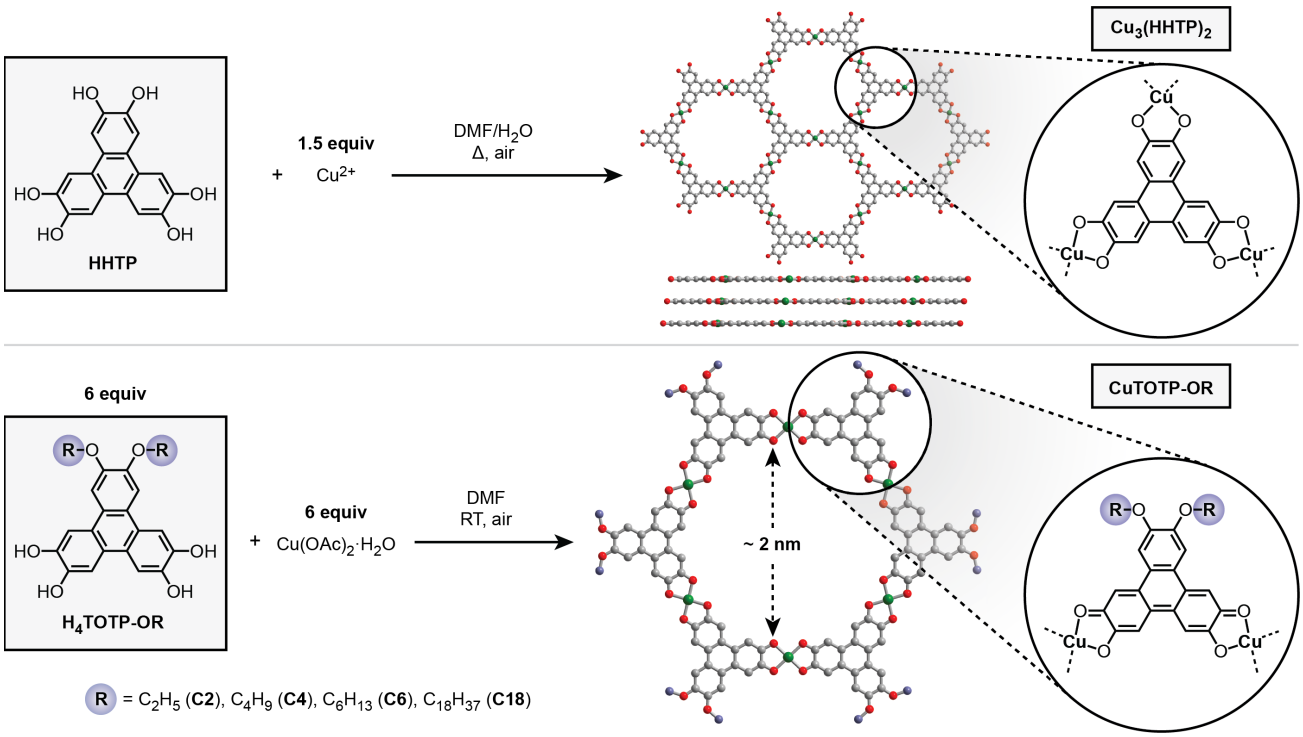

Figure 1. *Top:* Synthesis and structure of the 2D conductive metal–organic framework $Cu_3(HHTP)_2$. The material adopts a 2D honeycomb structure with a slipped π–π stacking arrangement between layers (ref. 43). *Bottom:* Overview of our synthetic strategy to truncate $Cu_3(HHTP)_2$ into discrete copper-based macrocycles CuTOTP-OR (R = C2, C4, C6, C18).

Results and discussion.

Synthesis and structure. Our overall synthetic strategy towards fully conjugated, planar metal–organic macrocycles is outlined in **Fig. 1**. To preserve extended π–d conjugation, each Cu^{2+} metal center is bridged by planar triphenylene-based ligands that closely resemble HHTP (HHTP = 2,3,6,7,10,11-hexahydroxytriphenylene), a tritopic linker commonly used to construct conductive 2D MOFs like $Cu_3(HHTP)_2$.[33] However, because one of the three catechol units is intentionally capped with alkyl groups, the formation of an extended network is instead truncated into 0D, planar macrocycles. This approach was inspired by recent work from Dichtel, Northrup, and coworkers, who used a similar strategy to achieve boronate ester-based macrocycles that are structurally reminiscent of 2D covalent organic frameworks.[24,34]

Combining the tetrahydroxytriphenylene ligands shown in **Fig. 1**, which we have abbreviated H_4TOTP-OR ($TOTP^{n-}$ = 2,3,6,7-**t**etra**o**xido**t**ri**p**henylene, R = alkyl group), with $Cu(OAc)_2{\cdot}H_2O$ in dimethylformamide (DMF) under air readily produces the desired copper-based macrocycles CuTOTP-OR in excellent yields (67–88% yield). To probe the influence of peripheral functionalization on macrocycle structure, packing, and solution processability, we further synthesized a family of four macrocycles that differ only in the length of the capping linear alkyl chain (R = C2, C4, C6, and C18).

Powder X-ray diffraction (PXRD) patterns of the resulting dark blue-black solids show three prominent low-angle peaks with a 1:1/√3:1/2 ratio in d-spacing, consistent with hexagonal packing (**Fig. 2a**). A broader feature at higher angles, which we have assigned as the (001) reflection, reveals a short interlayer distance of ~3.20 Å. This value is nearly identical to what has been observed in structurally

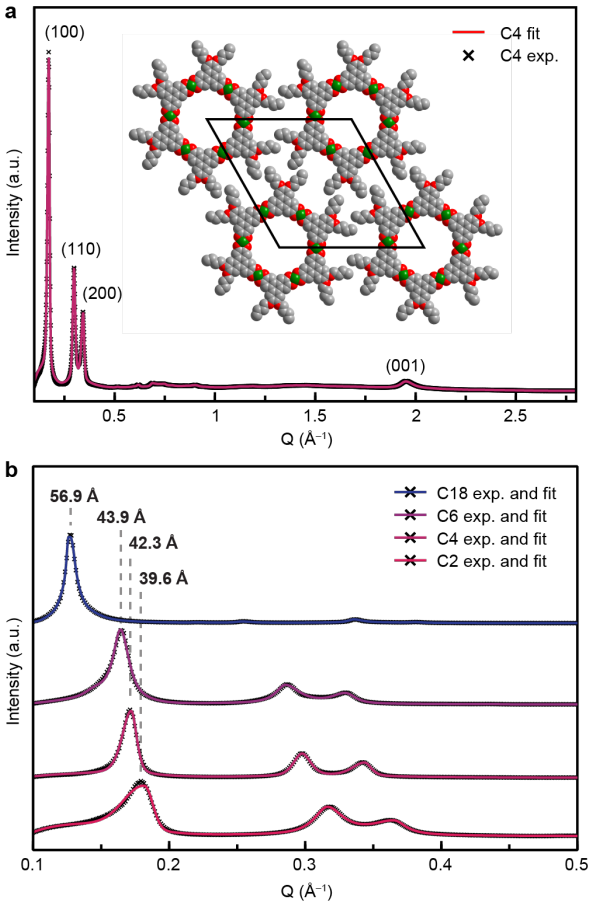

Figure 2. (a) PXRD pattern of DMF-solvated CuTOTP-OC4 and optimized structural model. (b) PXRD patterns and peak positions for DMF-solvated CuTOTP-OR.

related copper-based 2D metal–organic frameworks (3.19 Å) and is indicative of strong π–π stacking interactions between the planar macrocycles.[35] The broadness of the (001) peak suggests poor long-range ordering in the π-stacking *c* direction. In addition to a perfectly eclipsed arrangement between stacked macrocycles, numerous translational and rotational displacements are also possible. Further work and more crystalline materials are needed to accurately determine the preferred π–π stacking pattern in these materials.

Pawley refinements were performed to obtain more precise unit cell dimensions of DMF-solvated CuTOTP-OR (**Figs. S1–S4**). As expected, the in-plane lattice parameter systematically increases as the peripheral alkyl chains lengthen ($a = b$ = 40–57 Å), while the interlayer distance remains relatively constant (c = 3.20–3.24 Å) (**Fig. 2b**). Geometry optimized structural models afford similar unit cell dimensions (**Fig. S5** and **S6**). Transmission electron microscopy (TEM) images of CuTOTP-OC4 drop-cast from dilute solutions reveal average diameters of 1.9(4) nm, consistent with the expected size of the planar macrocyclic core (**Fig. S7**). Atomic force microscopy (AFM) images of more concentrated CuTOTP-OC4 solutions (1 mg mL^{-1}) clearly show the formation of nanotubular structures, with an average length of 23(6) nm (**Fig. S9**). No porosity was observed via traditional 77 K N_2 adsorption experiments, likely due to partial pore blockage by neighboring alkyl chains. However, similar measurements at 195 K using CO_2, a smaller probe molecule, led to a surface area of 226(3) m^2/g for CuTOTP-OC2. Altogether, the data obtained from PXRD, TEM, AFM, and gas sorption measurements are fully consistent with the columnar stacking of hexagonal macrocycles to form large nanochannels of approximately 2 nm in diameter.

Compared to extended 2D MOFs, the long-range structure of CuTOTP-OR is considerably more dynamic. In particular, the weak noncovalent interactions between neighboring alkyl chains are readily perturbed by solvent. While the interlayer distance stays relatively constant, reversible expansions and contractions in the *ab* plane are observed upon altering the macrocycle solvation state (**Table 1**). For example, the in-plane lattice parameter of fully dried CuTOTP-OC4 increases by >5% upon DMF solvation, suggesting partial solvent infiltration between the columnar stacks.

Table 1. Lattice parameters of CuTOTP-OR macrocycles in dried and DMF-solvated states.

CuTOTP-OR	Dry		DMF-Solvated	
	a* = *b (Å)	***c*** (Å)	***a* = *b*** (Å)	***c*** (Å)
R = C2	38.46(3)	3.19(1)	39.56(2)	3.22(1)
R = C4	40.16(2)	3.17(1)	42.30(2)	3.23(1)
R = C6	42.93(2)	3.17(1)	43.89(2)	3.20(1)
R = C18	55.86(6)	3.21(1)	56.91(2)	3.24(1)

We hypothesized that by tuning both the solvent identity and macrocycle peripheral functionalization, we should be able to fully separate the individual columnar stacks and achieve stable colloidal dispersions. With sonication, average particle sizes of around 90, 200, and 300 nm were observed by dynamic light scattering (DLS) for THF-dispersed CuTOTP-OC2, C4, and C6, respectively. However, these dispersions were not stable and further aggregation was observed over time. In contrast, dispersions of CuTOTP-OC18 in THF appear indefinitely stable across all concentrations tested (up to 10 mg/mL). Furthermore, DLS measurements revealed an average hydrodynamic diameter of 5(1) nm, consistent with short, isolated columnar stacks of macrocycles. Similar diameters (4–5 nm) were also observed in other organic solvents, such as $CHCl_3$ and toluene (**Table S1**). The ease by which CuTOTP-OR forms high concentration inks may afford future processability advantages relative to traditional metal–organic frameworks.

Spectroscopic characterization. Depending on the synthesis conditions, significant Cu(II)/Cu(I) mixed valency has been observed in the copper-based 2D frameworks $Cu_3(HHTP)_2$ and $Cu_3(HITP)_2$ (HITP = 2,3,6,7,10,11-hexaiminotriphenylene).[36] To determine whether similar mixed valency is observed in CuTOTP-OR, we probed the metal oxidation state using Cu K-edge X-ray absorption near-edge spectroscopy (XANES) (**Fig. 3**). The edge energy (as defined by the first peak of the first derivative spectra) is typically around 8981 eV for Cu(I) and 8985 eV for Cu(II) compounds.[37] The XANES spectra of all four CuTOTP-OR materials (R = C2, C4, C6, C18) were nearly identical, with edge energies between 8985–8986 eV (**Fig. 3** and **Fig. S11**). Overall, the observed XANES spectral features, the simple first-neighbor only extended X-ray absorption fine structure (EXAFS) oscillations, and the average Cu–O bond lengths obtained from EXAFS fitting ($d_{Cu–O}$ = 1.94(1) Å, see **Table S2**) are very similar to $Cu(acac)_2$ ($acac^{1-}$ = acetylacetonate) and other reference compounds containing square planar Cu(II) centers **(Figs. S10–S13).**[38]

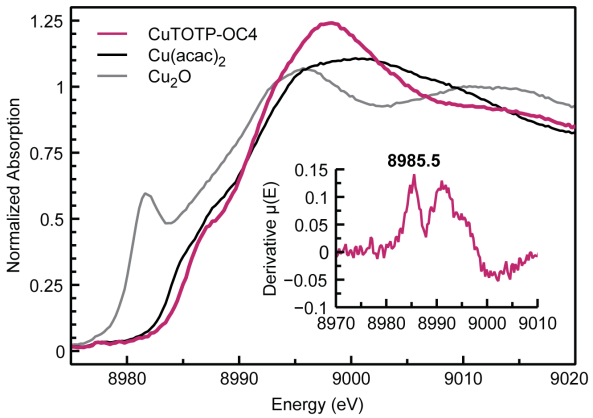

Figure 3. XANES spectra of CuTOTP-OC4 (purple) compared to reference Cu_2O (gray) and $Cu(acac)_2$ (black) compounds. *Inset*: Derivative spectra of CuTOTP-OC4, showing a first peak at 8985.5 eV.

High-resolution X-ray photoelectron spectroscopy (XPS) measurements of the Cu 2p region were carried out to further corroborate our Cu(II) assignment (**Fig. S15**). The Cu $2p_{3/2}$ peak of Cu(II) compounds is characterized by multiplet broadening and strong satellite features at higher binding energies.[39,40] In contrast, the Cu $2p_{3/2}$ peak of Cu(I) compounds is narrower and displays a very weak shake-up satellite. By comparing the relative areas of the main $2p_{3/2}$ peak and the shake-up satellite, we estimate that ≥90% of the copper centers in CuTOTP-OR are in the +2 oxidation state (see **Table S6** and the Supporting Information for more analysis details). We note that the complexity of Cu 2p XPS spectra can introduce large errors (±15%) in curve-fitting and quantification.[40] Nevertheless, taken together, our XANES and XPS data provide strong support for a predominantly Cu(II) oxidation state assignment.

After establishing the metal oxidation state in CuTOTP-OR, we next turned to the ligand. The two redox-active dioxolene units present in H_4TOTP-OR can each adopt three distinct redox states: the dianionic catecholate (cat^{2-}), monoanionic semiquinone (sq^{1-}), and neutral quinone (q^0) (**Fig. 4a**). These three states are readily distinguished by infrared spectroscopy. As the dioxolene unit is sequentially oxidized, its C–O stretching frequency (ν_{C-O}) systematically increases. In general, metal–catecholate, semiquinone, and quinone complexes display ν_{C-O} bands between 1250–1275, 1400–1500, and 1630–1640 cm^{-1}, respectively.[41] The infrared spectrum of CuTOTP-OC4 displays a strong feature at 1430 cm^{-1}, consistent with a metal–semiquinone C–O stretch (**Fig. 4b**). A band at 1246 cm^{-1} is also observed, which we have assigned as the ν_{C-O} of the alkyl-capped catechol unit. Similar features are also observed in the other alkyl variants of CuTOTP-OR (**Fig. S16**). Based on the infrared spectra, we propose the ligand is aerobically oxidized during synthesis to the dianionic TOTP-OR^{2-} form, where the bridging dioxolene units are in the $[sq, sq]^{2-}$ state.

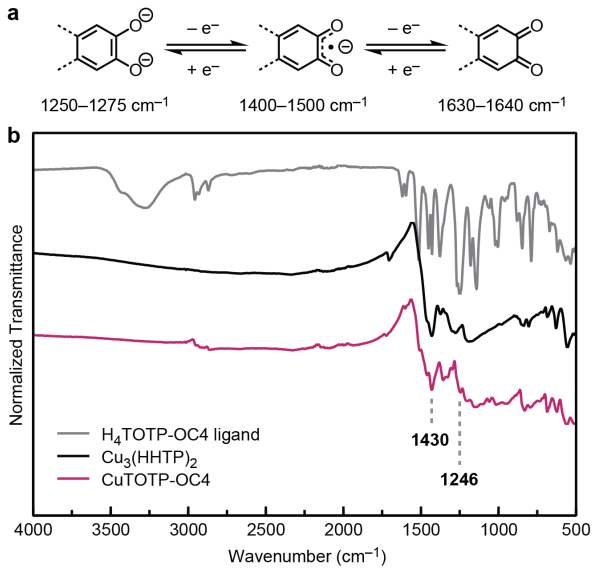

Figure 4. (a) Characteristic ν_{C-O} bands for metal–catecholate, semiquinone, and quinone complexes. (b) Infrared spectra of the H_4TOTP-OC4 ligand, $Cu_3(HHTP)_2$ framework, and CuTOTP-OC4 macrocycle shown in gray, black, and purple, respectively.

UV-vis electronic absorption spectra are also consistent with a semiquinone assignment. Metal–semiquinone complexes typically show an intense band at ~300 nm, assigned as an intraligand transition, as well as a broader band between 600–700 nm, assigned as a metal-to-ligand charge transfer (MLCT).[41] Indeed, the UV-vis spectra of CuTOTP-OC4 displays strong absorbances at both 317 and 598 nm (**Fig. S18**). Similar features are observed in the structurally related $Cu_3(HHTP)_2$ metal–organic framework (356 and 622 nm).

Both the macrocycle CuTOTP-OR and the metal–organic framework $Cu_3(HHTP)_2$ display a broad absorption >1600 cm^{-1} that is not observed in the parent H_4TOTP-OR or HHTP ligands (**Figs. 4b** and **S16**). In $Cu_3(HHTP)_2$, this feature has been attributed to a low-energy electronic transition, though its exact nature remains unclear.[36] Previously proposed assignments have included low-lying transitions of charge carriers as well as intervalence charge-transfer,[36] though the latter explanation is less likely for CuTOTP-OR, as no ligand or metal-based mixed valency appears to be present in these macrocycles. The broad electronic absorbance suggests a low activation energy for charge transport, motivating further study into the electrical conductivity of these materials.

Charge transport measurements. Two-point conductivity measurements were performed at room temperature on pressed pellets of CuTOTP-OR using a custom screw cell equipped with brass electrodes. Surprisingly, despite the truncated structure, pressed pellets of CuTOTP-OC2 (10^{-3} S cm^{-1}) are nearly as conductive as $Cu_3(HHTP)_2$ powders (10^{-3}–10^{-2} S cm^{-1}) (**Table 2, Table S7**, and **Fig. S19**).[8,43] Similar conductivity values of ~10^{-4} S cm^{-1} were obtained for the R = C4 and C6 variants. While the pellet conductivity of CuTOTP-OC18 is only 10^{-7} S cm^{-1} due to the presence of long, insulating alkyl chains, higher values should be possible in thin films with controlled alignment and morphology.[44,45]

Table 2. Average room temperature (298 K) conductivity values obtained from pressed pellets of CuTOTP-OR and either pressed pellets or single crystals of $Cu_3(HHTP)_2$.

Sample	Conductivity (S cm^{-1})
CuTOTP-OC2[a]	$2(1) \times 10^{-3}$
CuTOTP-OC4[a]	$6(2) \times 10^{-4}$
CuTOTP-OC6[a]	$4(1) \times 10^{-4}$
CuTOTP-OC18[a]	$1(1) \times 10^{-7}$
$Cu_3(HHTP)_2$ (pellet)[b]	10^{-3}–10^{-2}
$Cu_3(HHTP)_2$ (single crystal, out-of-plane)[c]	1.5

[a]Average of three measurements. [b]Average conductivity obtained in this work is $6(2) \times 10^{-3}$ S cm^{-1}; previously reported values tabulated in ref. 8 range between 10^{-3} to 10^{-2} S cm^{-1}. [c]Value obtained from ref. 43.

Due to similarities in their structural, spectroscopic, and bulk conductivity properties, the CuTOTP-OR macrocycles provide a rare window into the out-of-plane charge transport properties of $Cu_3(HHTP)_2$ and related 2D conductive frameworks. As described in a recent review by Dincă and coworkers, many uncertainties still remain concerning the charge carrier type, carrier concentration, and carrier mobility in conductive MOFs.[8] For example, the nature of the charge carriers (electrons or holes) in $Cu_3(HHTP)_2$ is still under debate. Recent thermoelectric measurements suggest $Cu_3(HHTP)_2$ is an n-type semiconductor,[46] while previous field-effect transistor (FET) devices point towards p-type transport.[42]

Solution-processable metal–organic macrocycles are amenable to characterization techniques routinely employed by the organic semiconductor community but challenging to access with traditional porous solids. To probe the charge carrier identity and mobility, thin-film field-effect transistors were fabricated using the CuTOTP-OC18 macrocycles as the transport layer. The detailed results of FET characterization are shown in the Supporting Information and sample transfer curves are shown in **Fig. S20**. All measurements were performed under an N_2 atmosphere. Interestingly, the FETs displayed ambipolar behavior, producing comparable hole and electron mobilities. The average saturation hole mobility ($\mu_{h,sat}$) was $(6.17 \pm 0.51) \times 10^{-3}$ cm^2 V^{-1} s^{-1} and the average saturation electron mobility ($\mu_{e,sat}$) was $(2.16 \pm 0.61) \times 10^{-3}$

$cm^2\ V^{-1}\ s^{-1}$. The voltage thresholds were –50 V and 30 V, respectively, and the on/off drain current ratio was on the order of 10^4. We note that the CuTOTP-OC18 devices were not exhaustively optimized, and it is likely that higher mobilities could be achieved by tuning various parameters, such as the casting solution concentration, deposition spin rate, and device layer interface.

Given the strong structural resemblance between CuTOTP-OR and $Cu_3(HHTP)_2$, these results suggest that $Cu_3(HHTP)_2$ may similarly display ambipolar conduction in the out-of-plane direction. While ambipolar transport has been previously reported in the thiolate-based 2D framework $Cu_3(C_6S_6)$,[47] to the best of our knowledge it has not been observed in $Cu_3(HHTP)_2$ or any other semiquinone-based 2D metal–organic framework.[8] Together, these studies show how discrete, solution-processable macrocycles can provide deeper insight into the charge transport properties of 2D conductive frameworks.

Electrochemical characterization. The concentration of charge carriers and the overall conductivity of semiconducting polymers and metal–organic frameworks can be tuned across many orders of magnitude through simple oxidative (p-type) and reductive (n-type) doping.[48–53] Motivated by these previous studies, we were interested in understanding whether our macrocycles, which contain redox-active ligands (**Fig. 4a**), are stable to further chemical reduction or oxidation. We hypothesized that the large interior channels present in CuTOTP-OR should be able to accommodate the insertion of charge-balancing ions without perturbing the π–π stacking pathways critical for charge transport.

To probe the redox properties of our macrocycles, solid-state cyclic voltammograms (CVs) of CuTOTP-OC2 were collected in 0.05 M $NaClO_4$ in acetonitrile. Working electrodes were prepared by dropcasting CuTOTP-OC2 dispersed in THF on glassy carbon electrodes. A representative CV of CuTOTP-OC2 is shown in **Fig. 5**. The compound displays quasi-reversible reduction events at $E_{1/2}$ = –0.20 V and –0.66 V vs. Fc^+/Fc. In contrast to the relative reductive stability, scanning to more positive potentials than ~0 V vs Fc^+/Fc led to irreversible oxidative features indicative of either macrocycle decomposition or loss of electrical contact with the electrode. While a comprehensive study is outside the scope of this work, these preliminary CV experiments suggest that reductive doping may be a promising avenue to tune the charge transport properties of CuTOTP-OR.

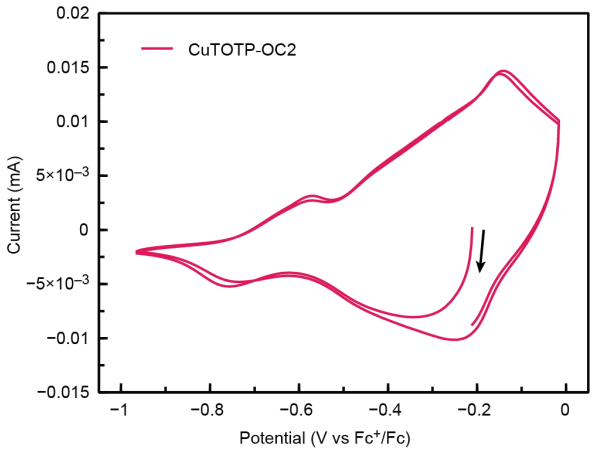

Figure 5. Solid-state cyclic voltammogram (2 cycles) of CuTOTP-OC2 collected at 10 mV s^{-1} in 0.05 M $NaClO_4$ in acetonitrile. The arrow indicates the direction of the forward scan.

Conclusion. The planar metal–organic macrocycles described here, which readily π-stack to form 1D columns, occupy a rare space in between molecules and materials. Going forward, CuTOTP-OR represents an important model system for understanding how magnetic and electronic interactions evolve as individual MOF layers self-assemble into π-stacked materials. More broadly, conjugated metal–organic macrocycles can serve as a bridge between 'hard' inorganic porous materials and 'soft' organic polymers. Future work will focus on how structural modifications across length scales influence electronic and ionic transport in this new class of soft nanoporous semiconductors.

ASSOCIATED CONTENT

Supporting Information

Additional experimental details, synthetic procedures, and characterization data (PXRD, XAS, XPS, EPR, UV-Vis, and NMR). The Supporting Information is available free of charge on the ACS Publications website.

Supporting Information (PDF)

AUTHOR INFORMATION

Corresponding Author

* Dianne J. Xiao – Department of Chemistry, University of Washington, Seattle, Washington 98195-1700, United States
Email: djxiao@uw.edu

Author Contributions

The manuscript was written through contributions of all authors. All authors have given approval to the final version of the manuscript.

Funding Sources

NSF: DMR-1719797
DOE: DE-SC0021966
DOE: DE-SC0019911
DOE: DE-SC0019288

ACKNOWLEDGMENT

Initial synthetic efforts were supported by the University of Washington (startup funds) and the NSF through a seed grant from the University of Washington Materials Research Science and Engineering Center DMR-1719797. Subsequent materials characterization by L.B.Z. was supported by the U.S. Department of Energy, Office of Science, Office of Basic Energy Sciences under Award Number DE-SC0021966. L.G., who performed the FET mobility measurements, was supported by the Department of Energy Office of Basic Energy Sciences under award number DE-SC0019911. D.D., who carried out the XAS measurements and analysis, was supported in part by the Joint Center for Energy Storage Research (JCESR), an Energy Innovation Hub funded by the U.S. Department of Energy, Office of Science, Basic Energy Sciences. M.M., who carried out the TEM measurements, was supported by the U.S. Department of Energy, Office of Science, Office of Basic Energy Sciences DE-SC0019288. L.B.Z., A.A.K, and D.D. were supported in part by the state of Washington through graduate fellowships from the University of Washington Clean Energy Institute.

The authors acknowledge the use of instrumentation at the following shared facilities: the Washington Research Training Testbeds, a facility operated by the University of Washington Clean Energy Institute; the University of Washington Photonics

Center; the Molecular Analysis Facility, a National Nanotechnology Coordinated Infrastructure (NNCI) site at the University of Washington, which is supported in part by funds from the National Science Foundation (awards NNCI-2025489, NNCI-1542101), the Molecular Engineering & Sciences Institute, and the Clean Energy Institute; and the MEM-C shared facilities, supported by the U.S. National Science Foundation through the UW Molecular Engineering Materials Center (MEM-C), a Materials Research Science and Engineering Center (DMR-171797). This research also used the mail-in program at Beamline 17-BM of the Advanced Photon Source, a U.S. Department of Energy (DOE) Office of Science User Facility, operated for the DOE Office of Science by Argonne National Laboratory under Contract No. DE-AC02-06CH11357. Finally, we gratefully acknowledge easyXAFS for assistance collecting EXAFS measurements, Dr. Samantha Young for assistance collecting and analyzing XPS data, Dr. Heather Niles for assistance collecting and analyzing AFM data, and Dr. Michael E. Ziebel for helpful scientific discussions.

REFERENCES

(1) Yang, Z.; Ren, J.; Zhang, Z.; Chen, X.; Guan, G.; Qiu, L.; Zhang, Y.; Peng, H. Recent Advancement of Nanostructured Carbon for Energy Applications. *Chem. Rev.* **2015**, *115* (11), 5159–5223. https://doi.org/10.1021/cr5006217.

(2) Wang, L.; Han, Y.; Feng, X.; Zhou, J.; Qi, P.; Wang, B. Metal–Organic Frameworks for Energy Storage: Batteries and Supercapacitors. *Coordination Chemistry Reviews* **2016**, *307*, 361–381. https://doi.org/10.1016/j.ccr.2015.09.002.

(3) Liang, Z.; Qu, C.; Guo, W.; Zou, R.; Xu, Q. Pristine Metal-Organic Frameworks and Their Composites for Energy Storage and Conversion. *Adv. Mater.* **2018**, *30* (37), 1702891. https://doi.org/10.1002/adma.201702891.

(4) Meng, Z.; Stolz, R. M.; Mendecki, L.; Mirica, K. A. Electrically-Transduced Chemical Sensors Based on Two-Dimensional Nanomaterials. *Chem. Rev.* **2019**, *119* (1), 478–598. https://doi.org/10.1021/acs.chemrev.8b00311.

(5) Stassen, I.; Burtch, N.; Talin, A.; Falcaro, P.; Allendorf, M.; Ameloot, R. An Updated Roadmap for the Integration of Metal–Organic Frameworks with Electronic Devices and Chemical Sensors. *Chem. Soc. Rev.* **2017**, *46* (11), 3185–3241. https://doi.org/10.1039/C7CS00122C.

(6) Mendecki, L.; Ko, M.; Zhang, X.; Meng, Z.; Mirica, K. A. Porous Scaffolds for Electrochemically Controlled Reversible Capture and Release of Ethylene. *J. Am. Chem. Soc.* **2017**, *139* (48), 17229–17232. https://doi.org/10.1021/jacs.7b08102.

(7) Voskian, S.; Hatton, T. A. Faradaic Electro-Swing Reactive Adsorption for CO_2 Capture. *Energy Environ. Sci.* **2019**, *12* (12), 3530–3547. https://doi.org/10.1039/C9EE02412C.

(8) Xie, L. S.; Skorupskii, G.; Dincă, M. Electrically Conductive Metal–Organic Frameworks. *Chem. Rev.* **2020**, *120* (16), 8536–8580. https://doi.org/10.1021/acs.chemrev.9b00766.

(9) Forrest, S. R. The Path to Ubiquitous and Low-Cost Organic Electronic Appliances on Plastic. *Nature* **2004**, *428* (6986), 911–918. https://doi.org/10.1038/nature02498.

(10) Sirringhaus, H.; Kawase, T.; Friend, R. H.; Shimoda, T.; Inbasekaran, M.; Wu, W.; Woo, E. P. High-Resolution Inkjet Printing of All-Polymer Transistor Circuits. *Science* **2000**, *290* (5499), 2123–2126. https://doi.org/10.1126/science.290.5499.2123.

(11) Root, S. E.; Savagatrup, S.; Printz, A. D.; Rodriquez, D.; Lipomi, D. J. Mechanical Properties of Organic Semiconductors for Stretchable, Highly Flexible, and Mechanically Robust Electronics. *Chem. Rev.* **2017**, *117* (9), 6467–6499. https://doi.org/10.1021/acs.chemrev.7b00003.

(12) Wang, S.; Oh, J. Y.; Xu, J.; Tran, H.; Bao, Z. Skin-Inspired Electronics: An Emerging Paradigm. *Acc. Chem. Res.* **2018**, *51* (5), 1033–1045. https://doi.org/10.1021/acs.accounts.8b00015.

(13) Matsuhisa, N.; Chen, X.; Bao, Z.; Someya, T. Materials and Structural Designs of Stretchable Conductors. *Chem. Soc. Rev.* **2019**, *48* (11), 2946–2966. https://doi.org/10.1039/C8CS00814K.

(14) Yang, Y.; Urban, M. W. Self-Healing Polymeric Materials. *Chem. Soc. Rev.* **2013**, *42* (17), 7446. https://doi.org/10.1039/c3cs60109a.

(15) Kang, J.; Tok, J. B.-H.; Bao, Z. Self-Healing Soft Electronics. *Nat Electron* **2019**, *2* (4), 144–150. https://doi.org/10.1038/s41928-019-0235-0.

(16) Hosono, N.; Kitagawa, S. Modular Design of Porous Soft Materials via Self-Organization of Metal–Organic Cages. *Acc. Chem. Res.* **2018**, *51* (10), 2437–2446. https://doi.org/10.1021/acs.accounts.8b00361.

(17) Moore, J. S. Shape-Persistent Molecular Architectures of Nanoscale Dimension. *Acc. Chem. Res.* **1997**, *30* (10), 402–413. https://doi.org/10.1021/ar950232g.

(18) Yamaguchi, Y.; Yoshida, Z. Shape-Persistency and Molecular Function in Heteromacrocycles: Creation of Heteroarenecyclynes and Arene–Azaarenecyclynes. *Chem. Eur. J.* **2003**, *9* (22), 5430–5440. https://doi.org/10.1002/chem.200305099.

(19) Höger, S. Shape-Persistent Macrocycles: From Molecules to Materials. *Chem. Eur. J.* **2004**, *10* (6), 1320–1329. https://doi.org/10.1002/chem.200305496.

(20) Zhang, W.; Moore, J. S. Shape-Persistent Macrocycles: Structures and Synthetic Approaches from Arylene and Ethynylene Building Blocks. *Angew. Chem. Int. Ed.* **2006**, *45* (27), 4416–4439. https://doi.org/10.1002/anie.200503988.

(21) Iyoda, M.; Yamakawa, J.; Rahman, M. J. Conjugated Macrocycles: Concepts and Applications. *Angew. Chem. Int. Ed.* **2011**, *50* (45), 10522–10553. https://doi.org/10.1002/anie.201006198.

(22) Gong, B.; Shao, Z. Self-Assembling Organic Nanotubes with Precisely Defined, Sub-Nanometer Pores: Formation and Mass Transport Characteristics. *Acc. Chem. Res.* **2013**, *46* (12), 2856–2866. https://doi.org/10.1021/ar400030e.

(23) Jin, Y.; Wang, Q.; Taynton, P.; Zhang, W. Dynamic Covalent Chemistry Approaches Toward Macrocycles, Molecular Cages, and Polymers. *Acc. Chem. Res.* **2014**, *47* (5), 1575–1586. https://doi.org/10.1021/ar500037v.

(24) Chavez, A. D.; Smith, B. J.; Smith, M. K.; Beaucage, P. A.; Northrop, B. H.; Dichtel, W. R. Discrete, Hexagonal Boronate Ester-Linked Macrocycles Related to Two-Dimensional Covalent Organic Frameworks. *Chem. Mater.* **2016**, *28* (14), 4884–4888. https://doi.org/10.1021/acs.chemmater.6b01831.

(25) Stang, P. J.; Persky, N. E.; Manna, J. Molecular Architecture via Coordination: Self-Assembly of Nanoscale Platinum Containing Molecular Hexagons. *J. Am.*

Chem. Soc. **1997**, *119* (20), 4777–4778. https://doi.org/10.1021/ja970537l.

(26) Leininger, S.; Olenyuk, B.; Stang, P. J. Self-Assembly of Discrete Cyclic Nanostructures Mediated by Transition Metals. *Chem. Rev.* **2000**, *100* (3), 853–908. https://doi.org/10.1021/cr9601324.

(27) Fujita, M.; Tominaga, M.; Hori, A.; Therrien, B. Coordination Assemblies from a Pd(II)-Cornered Square Complex. *Acc. Chem. Res.* **2005**, *38* (4), 369–378. https://doi.org/10.1021/ar040153h.

(28) Northrop, B. H.; Yang, H.-B.; Stang, P. J. Coordination-Driven Self-Assembly of Functionalized Supramolecular Metallacycles. *Chem. Commun.* **2008**, No. 45, 5896. https://doi.org/10.1039/b811712h.

(29) Frischmann, P. D.; Guieu, S.; Tabeshi, R.; MacLachlan, M. J. Columnar Organization of Head-to-Tail Self-Assembled Pt_4 Rings. *J. Am. Chem. Soc.* **2010**, *132* (22), 7668–7675. https://doi.org/10.1021/ja910886g.

(30) Hu, Y.-X.; Hao, X.; Xu, L.; Xie, X.; Xiong, B.; Hu, Z.; Sun, H.; Yin, G.-Q.; Li, X.; Peng, H.; Yang, H.-B. Construction of Supramolecular Liquid-Crystalline Metallacycles for Holographic Storage of Colored Images. *J. Am. Chem. Soc.* **2020**, *142* (13), 6285–6294. https://doi.org/10.1021/jacs.0c00698.

(31) Acharyya, K.; Bhattacharyya, S.; Sepehrpour, H.; Chakraborty, S.; Lu, S.; Shi, B.; Li, X.; Mukherjee, P. S.; Stang, P. J. Self-Assembled Fluorescent Pt(II) Metallacycles as Artificial Light-Harvesting Systems. *J. Am. Chem. Soc.* **2019**, *141* (37), 14565–14569. https://doi.org/10.1021/jacs.9b08403.

(32) Sepehrpour, H.; Fu, W.; Sun, Y.; Stang, P. J. Biomedically Relevant Self-Assembled Metallacycles and Metallacages. *J. Am. Chem. Soc.* **2019**, *141* (36), 14005–14020. https://doi.org/10.1021/jacs.9b06222.

(33) Hmadeh, M.; Lu, Z.; Liu, Z.; Gándara, F.; Furukawa, H.; Wan, S.; Augustyn, V.; Chang, R.; Liao, L.; Zhou, F.; Perre, E.; Ozolins, V.; Suenaga, K.; Duan, X.; Dunn, B.; Yamamto, Y.; Terasaki, O.; Yaghi, O. M. New Porous Crystals of Extended Metal-Catecholates. *Chem. Mater.* **2012**, *24* (18), 3511–3513. https://doi.org/10.1021/cm301194a.

(34) Smith, M. K.; Powers-Riggs, N. E.; Northrop, B. H. Rational Synthesis of Bis(Hexyloxy)-Tetra(Hydroxy)-Triphenylenes and Their Derivatives. *RSC Adv.* **2014**, *4* (72), 38281–38292. https://doi.org/10.1039/C4RA06503D.

(35) Dou, J.-H.; Arguilla, M. Q.; Luo, Y.; Li, J.; Zhang, W.; Sun, L.; Mancuso, J. L.; Yang, L.; Chen, T.; Parent, L. R.; Skorupskii, G.; Libretto, N. J.; Sun, C.; Yang, M. C.; Dip, P. V.; Brignole, E. J.; Miller, J. T.; Kong, J.; Hendon, C. H.; Sun, J.; Dincă, M. Atomically Precise Single-Crystal Structures of Electrically Conducting 2D Metal–Organic Frameworks. *Nature Materials* **2021**, *20* (2), 222–228. https://doi.org/10.1038/s41563-020-00847-7.

(36) Stolz, R. M.; Mahdavi-Shakib, A.; Frederick, B. G.; Mirica, K. A. Host–Guest Interactions and Redox Activity in Layered Conductive Metal–Organic Frameworks. *Chem. Mater.* **2020**, *32* (18), 7639–7652. https://doi.org/10.1021/acs.chemmater.0c01007.

(37) Lamberti, C.; Bordiga, S.; Bonino, F.; Prestipino, C.; Berlier, G.; Capello, L.; D'Acapito, F.; Llabrés i Xamena, F. X.; Zecchina, A. Determination of the Oxidation and Coordination State of Copper on Different Cu-Based Catalysts by XANES Spectroscopy in Situ or in Operando Conditions. *Phys. Chem. Chem. Phys.* **2003**, *5* (20), 4502–4509. https://doi.org/10.1039/B305810G.

(38) Gaur, A.; Klysubun, W.; Nitin Nair, N.; Shrivastava, B. D.; Prasad, J.; Srivastava, K. XAFS Study of Copper(II) Complexes with Square Planar and Square Pyramidal Coordination Geometries. *Journal of Molecular Structure* **2016**, *1118*, 212–218. https://doi.org/10.1016/j.molstruc.2016.04.008.

(39) Biesinger, M. C. Advanced Analysis of Copper X-Ray Photoelectron Spectra. *Surface and Interface Analysis* **2017**, *49* (13), 1325–1334. https://doi.org/10.1002/sia.6239.

(40) Brundle, C. R.; Crist, B. V. X-Ray Photoelectron Spectroscopy: A Perspective on Quantitation Accuracy for Composition Analysis of Homogeneous Materials. *Journal of Vacuum Science & Technology A* **2020**, *38* (4), 041001. https://doi.org/10.1116/1.5143897.

(41) Vlček, A. Metal and Ligand Oxidation States in Dioxolene Complexes: Meaning, Assignment and Control. *Comments on Inorganic Chemistry* **1994**, *16* (4), 207–228. https://doi.org/10.1080/02603599408035860.

(42) Rubio-Giménez, V.; Galbiati, M.; Castells-Gil, J.; Almora-Barrios, N.; Navarro-Sánchez, J.; Escorcia-Ariza, G.; Mattera, M.; Arnold, T.; Rawle, J.; Tatay, S.; Coronado, E.; Martí-Gastaldo, C. Bottom-Up Fabrication of Semiconductive Metal-Organic Framework Ultrathin Films. *Adv. Mater.* **2018**, *30* (10), 1704291. https://doi.org/10.1002/adma.201704291.

(43) Day, R. W.; Bediako, D. K.; Rezaee, M.; Parent, L. R.; Skorupskii, G.; Arguilla, M. Q.; Hendon, C. H.; Stassen, I.; Gianneschi, N. C.; Kim, P.; Dincă, M. Single Crystals of Electrically Conductive Two-Dimensional Metal–Organic Frameworks: Structural and Electrical Transport Properties. *ACS Cent. Sci.* **2019**, *5* (12), 1959–1964. https://doi.org/10.1021/acscentsci.9b01006.

(44) Kaafarani, B. R. Discotic Liquid Crystals for Opto-Electronic Applications. *Chem. Mater.* **2011**, *23* (3), 378–396. https://doi.org/10.1021/cm102117c.

(45) Diao, Y.; Shaw, L.; Bao, Z.; Mannsfeld, S. C. B. Morphology Control Strategies for Solution-Processed Organic Semiconductor Thin Films. *Energy Environ. Sci.* **2014**, *7* (7), 2145–2159. https://doi.org/10.1039/C4EE00688G.

(46) de Lourdes Gonzalez-Juarez, M.; Flores, E.; Martin-Gonzalez, M.; Nandhakumar, I.; Bradshaw, D. Electrochemical Deposition and Thermoelectric Characterisation of a Semiconducting 2-D Metal–Organic Framework Thin Film. *J. Mater. Chem. A* **2020**, *8* (26), 13197–13206. https://doi.org/10.1039/D0TA04939E.

(47) Huang, X.; Sheng, P.; Tu, Z.; Zhang, F.; Wang, J.; Geng, H.; Zou, Y.; Di, C.; Yi, Y.; Sun, Y.; Xu, W.; Zhu, D. A Two-Dimensional π–d Conjugated Coordination Polymer with Extremely High Electrical Conductivity and Ambipolar Transport Behaviour. *Nat Commun* **2015**, *6* (1), 7408. https://doi.org/10.1038/ncomms8408.

(48) Wegner, G. Polymers with Metal-Like Conductivity—A Review of Their Synthesis, Structure and Properties. *Angew. Chem. Int. Ed. Engl.* **1981**, *20* (4), 361–381. https://doi.org/10.1002/anie.198103611.

(49) Heeger, A. J. Semiconducting and Metallic Polymers: The Fourth Generation of Polymeric Materials (Nobel Lecture). *Angew. Chem. Int. Ed.* **2001**, *40* (14), 2591–2611. https://doi.org/10.1002/1521-

3773(20010716)40:14<2591::AID-ANIE2591>3.0.CO;2-0.

(50) Kobayashi, Y.; Jacobs, B.; Allendorf, M. D.; Long, J. R. Conductivity, Doping, and Redox Chemistry of a Microporous Dithiolene-Based Metal–Organic Framework. *Chem. Mater.* **2010**, *22* (14), 4120–4122. https://doi.org/10.1021/cm101238m.

(51) Darago, L. E.; Aubrey, M. L.; Yu, C. J.; Gonzalez, M. I.; Long, J. R. Electronic Conductivity, Ferrimagnetic Ordering, and Reductive Insertion Mediated by Organic Mixed-Valence in a Ferric Semiquinoid Metal–Organic Framework. *J. Am. Chem. Soc.* **2015**, *137* (50), 15703–15711. https://doi.org/10.1021/jacs.5b10385.

(52) Xie, L. S.; Sun, L.; Wan, R.; Park, S. S.; DeGayner, J. A.; Hendon, C. H.; Dincă, M. Tunable Mixed-Valence Doping toward Record Electrical Conductivity in a Three-Dimensional Metal–Organic Framework. *J. Am. Chem. Soc.* **2018**, *140* (24), 7411–7414. https://doi.org/10.1021/jacs.8b03604.

(53) Aubrey, M. L.; Wiers, B. M.; Andrews, S. C.; Sakurai, T.; Reyes-Lillo, S. E.; Hamed, S. M.; Yu, C.-J.; Darago, L. E.; Mason, J. A.; Baeg, J.-O.; Grandjean, F.; Long, G. J.; Seki, S.; Neaton, J. B.; Yang, P.; Long, J. R. Electron Delocalization and Charge Mobility as a Function of Reduction in a Metal–Organic Framework. *Nature Mater* **2018**, *17* (7), 625–632. https://doi.org/10.1038/s41563-018-0098-1.

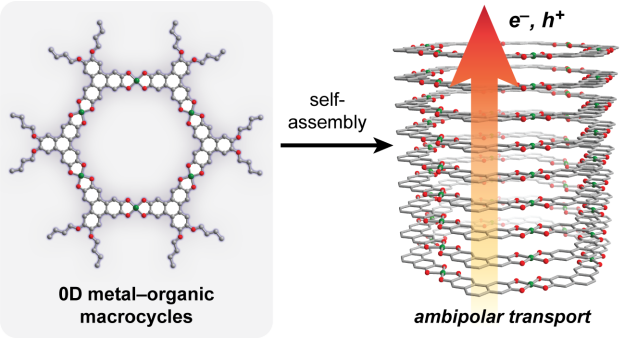
self-
assembly
e^-, h^+
0D metal–organic
macrocycles
ambipolar transport